Ducted Fan Noise Propagation Using Boundary Element Methods

C. Schram[1], M. Tournour[2]
[1] *LMS International, Belgium, Email: christophe.schram@lmsintl.com*
[2] *LMS International, Belgium, Email: michel.tournour@lmsintl.com*

Introduction

The noise produced by subsonic fans is a serious concern in a number of applications. Subsonic fans are for example involved in heating, ventilating and air-conditioning (HVAC) systems, and engine cooling systems. These are both characterized by quite complex geometries of the ducting that encloses the impeller. As a result, analytical methods based on tailored Green functions are irrelevant and the acoustic scattering must be computed numerically. The present work deals with the development and validation of accurate numerical methods for the prediction of subsonic fan noise in complex enclosures.

We focus on the role played by near-field terms in the acoustic scattering. Existing formulations, such as presented by Goldstein [1], discard explicitly the near-field terms. However, Roger [2] showed recently that the near-field terms can account for important phase-shifting effects, which can play a significant role, even in the amplitude of the acoustic far field, if for example the edge of a semi-infinite plane is present in the near field of the fan. This paper extends this analysis for the case of a ducted fan with different duct inlet geometries. The near-field formulation is implemented in a numerical acoustic solver to highlight the effect that a duct inlet geometry may have on restructuring near-field effects into propagating waves.

Test fan

The test fan which has a diameter of $D = 0.3$ m and a hub/tip ratio $\nu = 0.45$ is installed in a circular duct without guide vanes and rotates at $\Omega = 3000$ RPM. The Reynolds number, based on the chord length c of the blade and the mean relative flow velocity, varies from 118,000 at the hub to 178,000 at the tip. A grid type turbulence generator is installed $0.56D$ upstream of the impeller's leading edge plane, see Figure 1. The turbulence generator consists of six struts with a square cross-section of 0.015×0.015 m^2 and a separation distance of 0.06 m. Further details on the fan rig are given by Reese et al. [3].

Numerical strategy

The numerical method involves two steps. The first one consists in the simulation of the flow field around the rotating blades during their interaction with the stator wakes. In the second step, the forces exerted by the blades on the fluid are evaluated at frequencies equal to multiples of the rotation frequency (Blade Loading Harmonics, BLHs) and used as input of an aeroacoustic analogy implemented in a numerical acoustic solver.

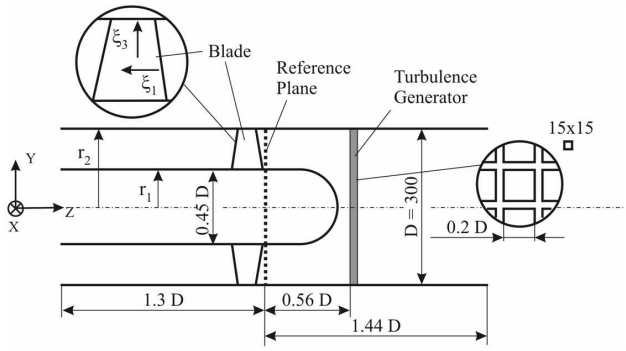

Figure 1: Fan assembly (main flow from right to left).

CFD modeling

The dominant dipole sound sources at the blade surfaces are predicted by an unsteady incompressible computational fluid dynamics (CFD) simulation. This simulation is carried out with a commercial flow solver [4], using the so-called Scale Adaptive Simulation (SAS) model. The unsteady flow field is solved with a second-order central difference scheme. The time integration is done by a second order backward Euler scheme.

In order to reduce the numerical costs only half of the impeller and the turbulence generator is meshed (Figure 2). This is possible because of the rotational symmetry of both components. The overall mesh size is 1.5 million hexahedral elements.

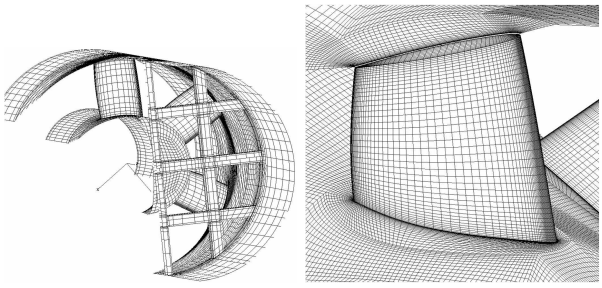

Figure 2: Numerical grid; left: complete grid (only every third gridline is plotted), right: detail of the grid near a fan blade.

The tip clearance is taken into account. The time increment is set such that 1,000 time steps correspond to one revolution of the impeller. A mass flow boundary condition is used at the inlet and the static pressure is set to zero at the outlet. For all remaining boundaries a no-slip wall condition is used. A more detailed description and a report of a validation with experimental data are given by Reese [3, 5].

Acoustic scattering

In this work, the sound production mechanism is described following the Ffowcs Williams and Hawkings approach [6], in which the unsteady flow effects are accounted for by equivalent sources distributed in the fluid and over a chosen control surface. The acoustic velocity field predicted by this method is used as a boundary condition of a Boundary Element Method or a Finite Element Method, in order to compute the acoustic scattering over the fan enclosure [7]. Summing the incident and scattered fields gives the acoustic field at a listener position located anywhere inside or outside of the duct system.

We restrict here the discussion to the tonal component of the sound spectrum, resulting from the periodic interaction of the fan blades with a flow field showing a mean spatial non-uniformity. Considering the loading noise component only (the quadrupole and thickness noise components are neglected at low Mach numbers), Goldstein [1] provides the far-field approximation of the acoustic field emitted, at the s^{th} Blade Passing Frequency Harmonic (BPFH), by a B-bladed rotor fan downstream of a stator with V vanes:

$$\rho_{sB} = -\frac{\mathrm{i}Bk_{sB}}{4\pi c_0^2}\,\frac{\mathrm{e}^{-\mathrm{i}k_{sB}x}}{x}\sum_{p=-\infty}^{+\infty}\mathrm{e}^{-\mathrm{i}\,(sB-pV)(\varphi-\pi/2)} \left(\mathrm{J}_{-sB+pV}(-k_{sB}r'\sin\theta)\,F_{pV}^{(T)}\cos\theta - \frac{sB-pV}{k_{sB}r'}\,\mathrm{J}_{-sB+pV}(-k_{sB}r'\sin\theta)\,F_{pV}^{(D)} - \mathrm{i}\,\mathrm{J}'_{-sB+pV}(-k_{sB}r'\sin\theta)\,\sin\theta\,F_{pV}^{(R)}\right) \quad (1)$$

where $k_{sB} = sB\Omega/c_0$ is the wavenumber of the s^{th} BPFH for a rotation pulsation Ω. c_0 is the speed of sound, (x, θ, φ) are the spherical coordinates of the listener and r' is the radius where the resulting blade force is applied, assuming a compact blade segment (see Figure 3). The Bessel function J_{-sB+pV} and its derivative account for the modulation of the frequency shift due to the Doppler effect. $F_p^{(X)}$ is the p^{th} Fourier component of the blade force $F_X(\tau)$ ($X = T, D, R$ denoting the thrust, drag and radial force components):

$$F_X(\tau) = \sum_{p=-\infty}^{\infty} F_p^{(X)}\,\mathrm{e}^{\mathrm{i}p\Omega\tau}\,.$$

In Equation (1) the contribution of the near-field terms is neglected, as well as the amplitude modulation in the retained far-field term. While these approximations are valid in the acoustical and geometrical far-field, it can argued that using (1) to calculate the incident field on a duct casing that is just adjacent to the blade tip could yield significant errors.

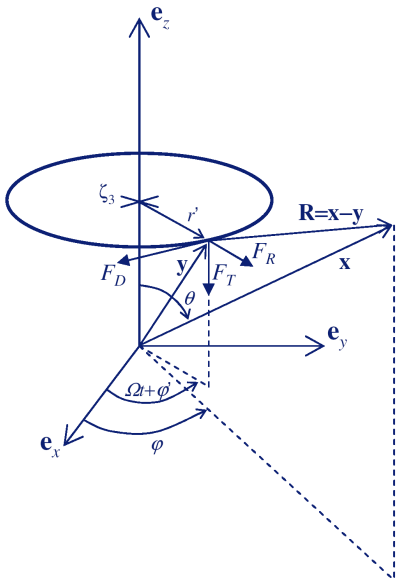

Figure 3: Fan coordinate system and force components.

If the near-field terms are retained, we obtain [2]:

$$\rho_{sB} = \frac{\mathrm{i}Bk_{sB}}{4\pi c_0^2}\sum_{p=-\infty}^{\infty} \left(-G_{sB-pV}^{(2)}\,F_{pV}^{(D)}\,x\,\sin\theta + G_{sB-pV}^{(3)}\,F_{pV}^{(R)}\,x\,\sin\theta + G_{sB-pV}^{(1)}\left(F_{pV}^{(T)}\,(\zeta_3 - x\,\cos\theta) - F_{pV}^{(R)}\,r'\right)\right) \quad (2)$$

with the Fourier components $G_m^{(N)}$ of the auxiliary Green's functions G_N ($N = 1, 2, 3$):

$$G_1(t) = \frac{\mathrm{e}^{-\mathrm{i}kR}}{R^2}\left(1 + \frac{1}{\mathrm{i}kR}\right)$$
$$G_2(t) = \sin(\Omega t + \varphi' - \varphi)\,G_1(t)$$
$$G_3(t) = \cos(\Omega t + \varphi' - \varphi)\,G_1(t)$$

are defined by:

$$G_N(\tau) = \sum_{m=-\infty}^{\infty} G_m^{(N)}\,\mathrm{e}^{\mathrm{i}m\Omega\tau}\,.$$

Results

A Boundary Element Method, implemented in a commercial software [7], is used to predict the sound field of the subsonic fan, and also to assess the effect of the duct inlet geometry. This permits assessing the importance of the near-field effects for a realistic geometry.

Free field radiation

The results displayed in Figure 4 were obtained assuming free field conditions. The listener is located over a circle with radius $r_l = 1$ m, centered on the fan and in its meridian plane.

The listener circle is interrupted over a downstream arc with 30 degrees width, where it would otherwise intersect

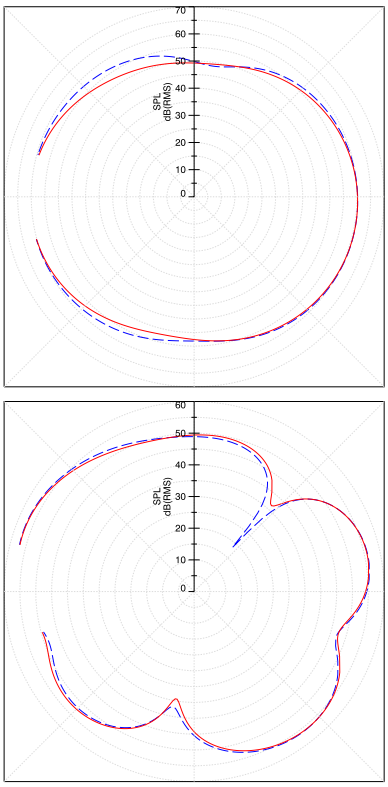

Figure 4: Free field directivities obtained using the far-field approximation (1) (solid red line) and the general solution (2) (dashed blue line) formulations. Up: first BPFH ($kr_d = 0.83$, $kr_l = 5.54$), bottom: fourth BPFH ($kr_d = 3.33$, $kr_l = 22.2$).

the duct walls for the ducted case. The results correspond to the first and fourth BPFHs of the fan, at frequencies equal to 300 Hz and 1200 Hz. The corresponding non-dimensional distances are $kr_l = 5.54$ and 22.2.

The results show that in free field, the predictions obtained using the far-field approximation and the general solution including near-field terms are quite close, even for the lowest frequency for which the listener is less than one wavelength apart from the fan center.

Ducted radiation

Good agreement between the prediction and the sound measurements, carried out at the University of Siegen, was reported in a previous paper [3]. In this work, numerical experiments are carried out in order to quantify the importance of the near-field terms in different configurations: the shape of the inlet mouth is varied by considering two fictitious geometries in addition to the baseline geometry (Figure 5): a flat-flanged inlet and a straight inlet.

The first results shown in Figure 6 highlight the importance of the near-field effects for the rounded flange and the straight inlet cases. At the first BPFH, the general solution (2) yields a directivity that is fairly similar to the one obtained with the far-field approximation (1) in the forward arc. In contrast, the results in the rear arc differ substantially, with a dip given by the far-field approximation (1) that is absent from the results given by the general solution (2). The differences are

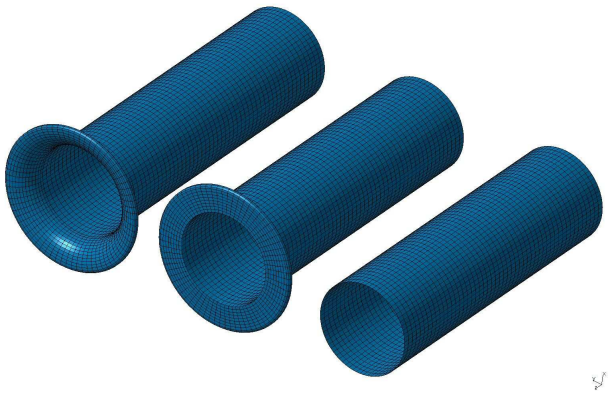

Figure 5: Geometrical configurations: rounded inlet (top), flat-flanged inlet (middle) and straight inlet (bottom).

more apparent for the fourth BPFH: for each geometry, discrepancies up to 10 dB are visible. Generally speaking, the far-field approximation yields directivities that are considerably more pronounced than the ones given by the general formulation.

Figure 7 shows the sensitivity of the sound field with regard to the duct geometry, respectively using the far-field approximation and the general formulation, for the fourth BPFH. These results demonstrate that the general formulation (2) indicates a smaller sensitivity to the geometry than the far-field approximation (1).

Conclusions

The accurate prediction of the tonal noise emitted by a low-subsonic fan relies on two main ingredients: the modeling of the force field exerted by the blades during their revolution, and the proper accounting of the scattering by the duct walls in general and by the duct inlet mouth in particular. A Computational Fluid Dynamics strategy based on transient simulations is adopted regarding the first aspect. A numerical approach is also proposed and validated for the acoustic part, which accounts for near-field effects in the calculation of the scattering by three different duct inlet geometries. The results demonstrate that while the near-field terms can be regarded as negligible for source-listener distances exceeding one wavelength in free field, these near-field effects can be significant, even in the acoustic far-field, when a scattering entity is located in the acoustic near-field of the fan. The general approach containing the near-field terms yields a directivity which is generally smoother than using the far-field approximation. This effect is more pronounced when the strength of the scattering is reinforced by geometrical singularities such as free edges or right-angled walls.

Acknowledgements

The authors acknowledge the kind support provided by Prof. Michel Roger for the derivation of the near-field expressions, as well as the contribution of Dr. Hauke Reese and Prof. Thomas Carolus, who provided the CFD calculations used in this work.

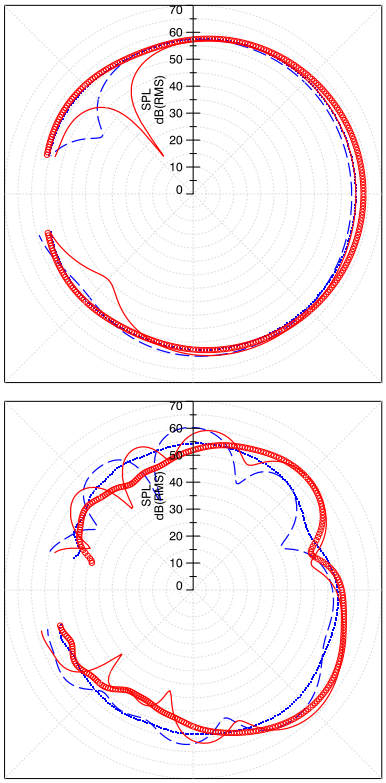

Figure 6: Effect of the near-field terms for the rounded flange and straight inlet cases. Solid red line: far-field formulation, rounded flange; red circles: general formulation, rounded flange; dashed blue line: far-field formulation, straight inlet; blue dots: general formulation, straight inlet. Up: first BPFH ($kr_d = 0.83$, $kr_l = 5.54$), bottom: fourth BPFH ($kr_d = 3.33$, $kr_l = 22.2$).

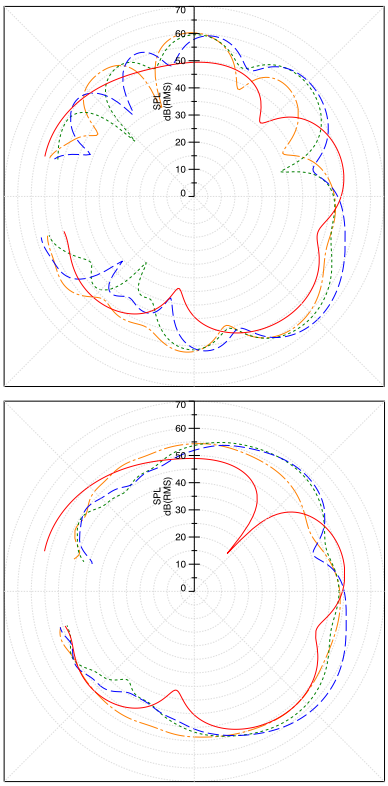

Figure 7: Effect of the ducting geometry, for the fourth BPFH. Solid red: free field; long dash blue: rounded flange; dotted green: flat flange; dash-dotted orange: no flange. Up: far-field approximation (1), bottom: general formulation (2).

References

[1] M. E. Goldstein. Aeroacoustics (1976). McGraw-Hill International Book Company.

[2] M. Roger. Near-field fan noise modelling and installation effects due to scattering surfaces. Fan Noise 2007, Lyon (2007), September 17–19.

[3] H. Reese and T. Carolus. Axial fan noise: towards sound prediction based on numerical unsteady flow data - a case study. Acoustics'08, Paris (2008), June 29 – July 4.

[4] ANSYS, Inc. CFX 10 User's Manual (2008).

[5] H. Reese. Anwendung von instationären numerischen simulationsmethoden zur berechnung aeroakustischer schallquellen bei axialventilatoren. Fortschr.-Ber. VDI Reihe **7**, Nr. 489 (2007), VDI Verlag. Düsseldorf.

[6] J. E. Ffowcs Williams and D. L. Hawkings. Sound generated by turbulence and surfaces in arbitrary motion. Philosophical Transactions of the Royal Society of London, Series A: Mathematical and Physical Sciences, **264**(1151) (1969), 321-342.

[7] LMS International. Virtual.Lab User's Guide (2008).